Coverage Analysis for Multi-Hop Communication in Intelligent-Surface-Assisted mmWave WLANs

Jingyuan Zhang
School of Electrical and Computer Engineering
Georgia Institute of Technology
Atlanta, Georgia, USA
jingyuan@ece.gatech.edu

Douglas M. Blough
School of Electrical and Computer Engineering
Georgia Institute of Technology
Atlanta, Georgia, USA
doug.blough@ece.gatech.edu

2023 IEEE 48th Conference on Local Computer Networks (LCN) | 979-8-3503-0073-4/23/$31.00 ©2023 IEEE | DOI: 10.1109/LCN58197.2023.10223314

***Abstract*—Reconfigurable intelligent surfaces (RISs) are an emerging technology to improve coverage in millimeter-wave bands, by providing reflective links between access points and user devices when line-of-sight (LoS) links are blocked. To understand the limits of multi-RIS coverage performance in mmWave wireless local area networks (WLANs), we employ stochastic geometry to analyze connection probability with both single-RIS and multi-RIS links with a sparse obstacle distribution. The connection probability for single-RIS links and an upper bound on connection probability for multi-RIS links are derived under an approximation where independence of LoS statuses of different links is assumed. Numerical simulations validate the analytical results and provide a comparison between single-RIS and multi-RIS links. Results demonstrate that single-RIS links provide substantial coverage increases for relatively short-distance communications but are not as effective for longer distances. Meanwhile, two-RIS links can provide substantially increased coverage for longer-range communications, but do not exhibit a significant advantage compared with single-RIS links for short distances.**

***Index Terms*—Millimeter-wave WLANs, intelligent surfaces, coverage probability, stochastic geometry, Poisson point process.**

I. Introduction

In recent years, millimeter-wave (mmWave) technology has received considerable attention in both academia and industry for fifth-generation (5G) and beyond communications due to the large bandwidth available at mmWave frequencies to fulfill the explosive demands of data services [1].

However, mmWave communication faces challenges including higher path loss and penetration loss compared with communication at lower frequencies, which can negatively impact communication performance and network coverage [1]. Proposed solutions to address the mmWave band coverage issue include multiple access point (AP) deployment [2], active amplify-and-forward relays or decode-and-forward relays [3] [4], passive reflectors [5] and reconfigurable intelligent surfaces (RISs) [6] [7]. Multi-AP deployment reduces "blind" spots by placing multiple APs to provide line-of-sight (LoS) links in regions that cannot be covered by a single AP, at the expense of increased power consumption and infrastructure complexity. Multi-antenna relays, passive reflectors and RISs all try to provide indirect links by retransmitting signals from the AP to the user when there is no LoS link between them. RISs are composed of an array of reflective electromagnetic elements, e.g. metallic or dielectric particles. Each of the RIS elements can be reconfigured in order to manipulate incident waves and obtain an arbitrary reflection angle. Therefore, RISs have the advantage of flexible beam configuration compared with passive reflectors and demonstrate benefits of low power consumption compared with multi-antenna relays [8].

Much existing work studies RIS phase configuration design to improve communication quality, e.g. [9] [10]. However, there is limited work to date on performance analysis of RIS-assisted networks, especially where multi-RIS links are included. In this paper, the connection probability[1] of both single-RIS and multi-RIS links are analyzed based on stochastic models, with the aim to characterize the obstacle tolerance of RIS-assisted networks. We consider a scenario with a single AP and randomly located RISs and obstacles, where obstacle density is not high. The relationships among coverage, RIS distribution, and obstacle distribution are studied to provide guidance for RIS deployment in mmWave wireless local area networks (WLANs) and a comparison between single-RIS and multi-RIS links is made to evaluate their relative benefits. Such a study is essential because signal sensitivity to obstacles is a primary concern for mmWave networks. In addition, analysis of multi-RIS links is necessary to determine whether it is worthwhile to use such links considering their extra overhead and delay due to routing and beam alignment among RISs.

The paper is organized as follows. Sec. II summarizes existing research on single-RIS and multi-RIS communication. Sec. III introduces preliminaries about stochastic geometry model and received power models for single-RIS and multi-RIS links, followed by system model in Sec. IV. Theoretical coverage analysis of single-RIS and multi-RIS links is presented in Sec. V and Sec. VI, respectively. Simulation results and comparison of coverage performance of single-RIS and multi-RIS links are provided in Sec. VII. Finally, Sec. VIII concludes the paper.

II. Related Work

RISs are a potential solution for mmWave band blockage, but it is important to analyze their performance through theory to improve network deployment and algorithm design. The authors in [11] theoretically analyze signal-to-noise ratio (SNR),

[1]We define connection probability as the probability that a user device can be connected to an AP via either a LoS link or an RIS-assisted link.

outage probability, average bit-error rate, and ergodic capacity of multi-RIS links with the assumption of independent double generalized Gamma fading channels, which does not explicitly model obstacles in the environment. Several papers employ stochastic geometry to explicitly model obstacle distribution in RIS-assisted networks (as we do herein as well). The authors in [12] analytically derive the probability that a single RIS can reflect the signal between a transmitter and receiver pair with the assumption that random obstacles are coated with RISs. However, important factors, including path loss model and received power to ensure communication quality, are not considered. In [13], the authors derive coverage probability for single-RIS links with a Boolean line model for obstacles and assuming some obstacles are coated with RISs. In their paper, the path loss is assumed to be proportional to $(r_1 + r_2)^{-\alpha}$, where α is the path-loss exponent, r_1 is the distance from transmitter to RIS, and r_2 is the distance from RIS to receiver. However, that path loss model assumes that the RIS path loss is similar to that of a passive reflector while still achieving the superior properties of an RIS, which does not comport with conclusions and measurements of the RIS path loss model from the literature [14].

In this paper, we adopt the well known far-field path loss model for RIS [14], where the far-field region is dependent on the RIS array size. Several recent papers show that there is only a small decrease in beamforming performance if a device is located in the Fresnel near-field compared with the case where the device is in traditionally defined far-field region [15] [16]. According to [15] [16], the Fresnel near-field is the region only a few meters away from the RIS array with 128×128 elements at mmWave band. It indicates that the far-field path loss is a reasonable approximation to use for network analysis, especially for indoor mmWave WLAN scenario.

To the best of the authors' knowledge, there is no prior research studying the impact of explicit obstacle distribution on coverage performance for both single-RIS and multi-RIS links in mmWave networks with realistic consideration of path loss model and signal strength. Moreover, the advantages of obstacle avoidance and coverage improvement that can be provided by multi-RIS links over single-RIS links in mmWave networks has not been addressed previously.

III. Preliminaries

Stochastic geometry is an analytical tool for evaluating network performance, where some important entities are randomly distributed in the desired region, typically according to a spatial Poisson point process (PPP) [17] [18]. Using stochastic geometry, critical network performance metrics including coverage probability and throughput can be derived via analytical expressions. This section provides background on stochastic geometry and received power model of RIS-assisted links which will be used to derived connection probability.

A. Stochastic geometry model

1) System setting for stochastic geometry: Based on a widely-used system setting of stochastic geometry, we consider a 2D case with one transmitter (TX), one receiver (RX) and randomly located obstacles as illustrated in Fig. 1. According to [17], obstacles can be modeled as random rectangles whose centers are modeled as PPP with density μ_o on a 2D plane. Obstacle length and width are typically assumed to be random variables with expectations $E(L)$ and $E(W)$, respectively. Moreover, the angle between the obstacle orientation and the positive direction of the x-axis is modeled as a random variable uniformly distributed between 0 and 2π.

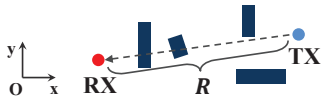

Fig. 1. Illustration of stochastic geometry model (Top view)

2) LoS probability based on stochastic geometry: LoS probability, which is the probability that there exists a LoS path connecting the TX and the RX, is an important metric, especially in mmWave communication where signals are extremely sensitive to blockage. When using the system setting described above, the LoS probability is given by [17]

$$P_{los}(R) = e^{-(\beta R + p)}, \tag{1}$$

where R is the horizontal distance between TX and RX, $\beta = \frac{2\mu_o(E(L)+E(W))}{\pi}$ and $p = \mu_o E(L)E(W)$.

B. Received power of RIS-assisted links

Considering that a user can establish a communication link to the AP if there is adequate received power, it is necessary to understand the received power model of RIS-assisted links. As mentioned earlier, we adopt the far-field path loss model for an RIS-aided link to analyze coverage performance. In what follows, let P_t denote the transmit power, λ denote the wavelength of the operational band, G_t and G_r represent the antenna gains at TX and RX, respectively, $G_{ris}(\theta)$ denote the gain of one RIS element, A denote the aperture of one RIS element, and N_k represent the number of elements on each RIS array. Herein, the free space path loss model is considered.

1) Received power of LoS links: The received power at RX is $P_{r,los} = P_t G_t G_r (\frac{\lambda}{4\pi R})^2$, where R is the LoS link length.

2) Received power of M-RIS links: Following [19], the received power of an M-RIS link, where the signal is sequentially reflected by M RISs before reaching the RX as shown in Fig. 2(a), can be modeled as:

$$P_{r,M} = P_t (N_k A)^{2M} \prod_{m=1}^{M+1} \frac{C'_m}{r_m^2}, \tag{2}$$

where r_m is the length of the mth segment in the indirect link as indicated in Fig. 2(a), and C'_m is related to the mth path segment. The value of C'_m is calculated as follows:

$$C'_m = \begin{cases} \dfrac{G_{ris}(\theta_{m,r})G_r}{4\pi}, & \text{if} \quad m = 1 \\ \dfrac{G_{ris}(\theta_{m,r})G_{ris}(\theta_{m,t})}{\lambda^2}, & \text{if} \quad 1 < m < M+1 \\ \dfrac{G_t G_{ris}(\theta_{m,t})}{4\pi}, & \text{if} \quad m = M+1 \end{cases}, \tag{3}$$

where $\theta_{m,r}$ and $\theta_{m,t}$ are the angle of reflection and angle of incidence of the wave interacting with the mth RIS.

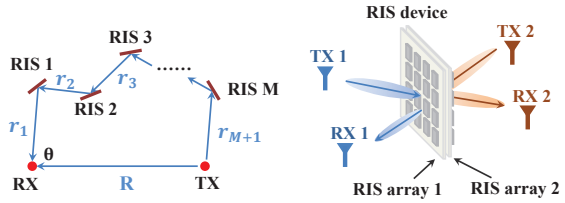

(a) M-RIS links

(b) RIS device with two back-to-back attached RIS arrays

Fig. 2. Illustration of RIS-assisted indirect link

IV. System Model

In this section, system model used for coverage analysis of multi-hop RIS link is introduced, followed by the definition of connection probabilities for RIS-assisted communication.

A. System model

In this paper, we consider a 2D scenario where there is a pair of transmitter and receiver at a distance of R, and the transmitter, the receiver, RIS devices, and obstacles are all placed in the same (X, Y) plane. Notably, the 2D model can serve as a foundational framework for exploring 3D scenarios where the transmitter, the receiver, and RIS devices are positioned at different heights. In this paper, it is assumed that each RIS device is equipped with two back-to-back attached RIS arrays as illustrated in Fig. 2(b). In other words, a communication link can be established if the transmitter and the receiver are located on the same side of the RIS device. It is also assumed that each RIS array is a square array with N_k RIS elements. For each RIS element, we adopt the standard assumption that the aperture is $A = \frac{\lambda}{2} \times \frac{\lambda}{2}$. Then, all RIS devices have length $L_r = \sqrt{N_k}\frac{\lambda}{2}$ and thickness W_r.

As described in Sec. III-A, locations of the centers of obstacles are modeled as a homogeneous PPP with density μ_o. Herein, we add a second homogeneous PPP with density μ_r to model the locations of centers of RIS devices. These two homogeneous PPPs are independent. The length L_o and width W_o of obstacles are uniformly distributed random variables with expectations of $E(L_o)$ and $E(W_o)$. The angle between any obstacle or RIS device and the positive direction of the x-axis is modeled as a uniform random variable between 0 and 2π. For tractability, it is assumed that the RIS element gain $G_{ris}(\theta)$ is a constant (independent of θ). The transmit power is denoted by P_t, and the minimum received power to support a communication link is denoted by $P_{r,th}$.

B. Definition of connection probabilities

In order to understand the coverage of RIS-aided systems, we analyze the connection probability, which represents the probability that the transmitter and the receiver can communicate through an unblocked link. We introduce two different definitions of connection probability as follows:

LoS connection probability, $P_0(R)$: the probability that there exists a LoS link between a transmitter and receiver pair at distance R with adequate received power at the receiver.

M-RIS connection probability, $P_M(D_M|R)$: the probability that there exists an M-RIS link to provide adequate received power at the receiver, given a transmitter and receiver pair at distance R, where D_M is a quantity that ensures the minimum received power to support the communication link is achieved and will be introduced later.

We further define the overall connection probability as: *Overall connection probability, $P_M(R)$:* the probability that there exists a LoS link or a multi-RIS link with at most M RISs that provides adequate received power at the receiver, given a transmitter and receiver pair at distance R.

1) LoS connection probability, $P_0(R)$: Different from the stochastic model introduced in Sec. III where only obstacles have impact on the LoS probability, RIS devices can also block signals. Considering that spatial distribution of obstacles and RIS devices are two independent PPPs, then the event that the LoS path between a pair of transmitter and receiver is blocked by obstacles and the event that the LoS path is blocked by RIS devices are independent. Therefore, according to Sec. III-A2, the LoS connection probability between a pair of transmitter and receiver with distance R is

$$P_{los}(R) = e^{-(\beta_o+\beta_r)R-(p_o+p_r)}, \tag{4}$$

where β_o, β_r, p_o, and p_r are given by

$$\beta_o = \frac{2\mu_o(E(L_o)+E(W_o))}{\pi}, \tag{5}$$

$$p_o = \mu_o E(L_o)E(W_o), \tag{6}$$

$$\beta_r = \frac{2\mu_r(L_r+W_r)}{\pi}, \tag{7}$$

$$p_r = \mu_r L_r W_r. \tag{8}$$

Since the transmitter can only communicate with receivers within its transmission range, the connection probability of LoS links is defined as

$$P_0(R) = \begin{cases} e^{-(\beta_o+\beta_r)R-(p_o+p_r)}, & \text{if} \quad r \le D_{los} \\ 0, & \text{if} \quad r > D_{los} \end{cases}, \tag{9}$$

where $D_{los} = \frac{\lambda}{4\pi}\sqrt{\frac{P_t G_t G_r}{P_{r,th}}}$ is the transmission range.

2) M-RIS connection probability, $P_M(D_M|R)$: To guarantee communication quality, the received power through an M-RIS link should be larger than a predefined threshold, such that $P_{r,M} \ge P_{r,th}$. Based on the received power model introduced in Sec. III-B2, the following condition should be met to ensure adequate received power at the receiver through an M-RIS link

$$\prod_{m=1}^{M+1} r_m \le \sqrt{\frac{P_t}{P_{r,th}}(N_k A)^{2M} \prod_{m=1}^{M+1} C'_m}. \tag{10}$$

For the ease of notation, the right side of Eq. (10) is denoted by D_M, so that $\prod_{m=1}^{M+1} r_m \le D_M$. Then $P_M(D_M|R)$ can be interpreted as the probability that there exists an unblocked M-RIS link where the product of $(M+1)$ segments in the path is less than or equal to D_M.

3) Approximated overall connection probability $\widehat{P_M}(R)$: An approximation of overall connection probability $P_M(R)$ is

$$\widehat{P_M}(R) = 1 - (1 - P_0(R)) \prod_{m=1}^{M} (1 - P_m(D_m|R)), \quad (11)$$

where dependencies between links with different numbers of RISs are ignored.

V. Connection probability of single-RIS links

In this section, the connection probability of single-RIS links is derived analytically. For simplicity, we assume that the polar coordinates of the transmitter and the receiver are $(\frac{R}{2}, 0)$ and $(\frac{R}{2}, \pi)$, respectively. The analysis of both single-RIS links in this section and multi-RIS links in the next section is based on an approximation that the numbers of obstacles on different links are independent, which implies that the LoS statuses of different links are independent. This is a good approximation for scenarios where obstacle distribution is not extremely dense and obstacles has relatively small sizes [13].

In this section, Lemma 3 shows the analytical results for connection probability of single-RIS links. Lemma 1 and Lemma 2 are used to provide preliminary conclusions used to derive Lemma 3.

Lemma 1 (Unblocked probability given RIS location): For a sparse obstacle distribution and a pair of transmitter and receiver with distance R, the probability that an RIS device with polar coordinate $\boldsymbol{q} = (r, \theta)$ can provide an unblocked single-RIS link between the transmitter and the receiver is approximated by

$$P_u(r, \theta|R) = H(r, \theta|R) \exp\Big(- (\beta_o + \beta_r)(r_1(r, \theta|R) + r_2(r, \theta|R)) - 2(p_o + p_r)\Big), \quad (12)$$

where

$$r_1(r, \theta|R) = \sqrt{r^2 + \frac{R^2}{4} + Rr\cos\theta}, \quad (13)$$

$$r_2(r, \theta|R) = \sqrt{r^2 + \frac{R^2}{4} - Rr\cos\theta}, \quad (14)$$

$$H(r, \theta|R) = 1 - \frac{1}{\pi}\cos^{-1}\Big(\frac{r_1^2(r, \theta|R) + r_2^2(r, \theta|R) - R^2}{2r_1(r, \theta|R)r_2(r, \theta|R)}\Big). \quad (15)$$

Proof 1: For the setup illustrated in Fig. 3, the conditions that a given RIS device can provide unblocked link includes the occurrence of the following three independent events: (1): there is a LoS link between RIS device and TX; (2) there is a LoS link between RIS device and RX; (3) the RIS device has a proper orientation so that TX and RX are on the same side of the RIS device.

The length of the link between RIS and RX $r_1(r, \theta|R)$ and the length of the link between RIS and TX $r_2(r, \theta|R)$ can be calculated by Law of Cosines to get the results in Eq. (13) and Eq. (14). Then the probability of occurrence of event (1) and (2) can be given based on Eq. (4) as $P_{los}(r_1(r, \theta|R))$ and $P_{los}(r_2(r, \theta|R))$, respectively.

For event (3), if the RIS device has the orientation as illustrated as RIS′ in Fig. 3, it cannot provide a proper single-RIS link since TX and RX are on different sides of the RIS device. The probability of event (3) occurring is

$$H(r, \theta|R) = 1 - \frac{\alpha}{\pi}, \quad (16)$$

where α is the angle between RX-RIS link and TX-RIS link and is given by

$$\alpha = \cos^{-1}\Big(\frac{r_1^2(r, \theta|R) + r_2^2(r, \theta|R) - R^2}{2r_1(r, \theta|R)r_2(r, \theta|R)}\Big). \quad (17)$$

Considering the independence of the three events, the unblocked probability given RIS device location is given by

$$P_u(r, \theta|R) = P_{los}(r_1(r, \theta|R))P_{los}(r_2(r, \theta|R))H(r, \theta|R). \quad (18)$$

Lemma 2 (Inhomogeneous PPP of unblocked RIS devices): For sparse obstacle distributions, RIS device locations that can provide an unblocked single-RIS link between a pair of transmitter and receiver with distance R are approximated by an inhomogeneous PPP denoted by $\Psi_{R,u}$ with density

$$\mu_{r,u} = \mu_r P_u(r, \theta|R). \quad (19)$$

Proof 2: Considering independence of LoS statuses of different links for sparse obstacle distributions, the ability of different RIS devices to provide unblocked single-RIS links is also independent. Therefore, the RIS device locations that can provide unblocked single-RIS links form a thinned Poisson process [2] generated from the original Poisson process of RIS device locations. Therefore, the density of the thinned process is $\mu_r P_u(r, \theta|R)$.

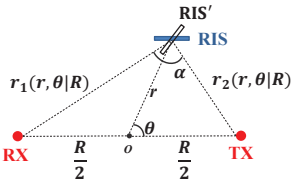

Fig. 3. Illustration of RIS orientation in a single-RIS link

Lemma 3 (Connection probability of single-RIS links): For a sparse obstacle distribution and a given pair of transmitter and receiver with distance R, connection probability of single-RIS links is approximated by

$$P_1(D_1|R) = \begin{cases} 1 - \exp\{-\mu_r \int_0^{2\pi}\int_0^{f(D_1,\theta|R)} P_u(r, \theta|R) r \mathrm{d}r\mathrm{d}\theta\}, & \text{if } R \le 2\sqrt{D_1} \\ 1 - \exp\{-2\mu_r \int_{-\theta_0(D_1|R)}^{\theta_0(D_1|R)}\int_{g(D_1,\theta|R)}^{f(D_1,\theta|R)} P_u(r, \theta|R) r \mathrm{d}r\mathrm{d}\theta\}, & \text{if } R > 2\sqrt{D_1} \end{cases}, \quad (20)$$

[2]Thinning a Poisson point process refers to classifying each point into a number of classes based on certain stochastic rule independently [20].

where D_1 is the threshold of the product of two path segments in single-RIS links, which is defined in Sec. IV-B2, and

$$f(D_1,\theta|R)=\frac{R}{2}\sqrt{\cos(2\theta)+\sqrt{16D_1^2/R^4-\sin^2(2\theta)}}, \quad (21)$$

$$g(D_1,\theta|R)=\frac{R}{2}\sqrt{\cos(2\theta)-\sqrt{16D_1^2/R^4-\sin^2(2\theta)}}, \quad (22)$$

$$\theta_0(D_1|R)=\frac{1}{2}\sin^{-1}(\frac{4D_1}{R^2}). \quad (23)$$

Proof 3: Let $\mathbf{q}=(r,\theta)$ denote RIS device locations, $r_1(r,\theta|R)$ and $r_2(r,\theta|R)$ denote the distance from RIS to RX and the distance from RIS to TX, respectively.

Based on Lemma 2, which defines the distribution of unblocked RIS devices, the connection probability of single-RIS links, $P_1(D_1|R)$, can be derived by the probability that there exists at least one RIS device from $\Psi_{R,u}$ defined in Lemma 2 whose location also satisfies the condition of $r_1(r,\theta|R)r_2(r,\theta|R)\le D_1$.

By using the conclusion of void probability of Poisson process, $P_1(D_1|R)$ can be derived by the probability that all the RIS device locations from $\Psi_{R,u}$ do not fall into the region defined as $\boldsymbol{S}=\{\boldsymbol{q}=(r,\theta)|r_1(r,\theta|R)r_2(r,\theta|R)\le D_1\}$. Then the connection probability of single-RIS links is given by

$$\begin{aligned}P_1(D_1|R)&=1-P(\mathbb{N}_{\Psi_{R,u}}(\boldsymbol{S})=0)\\&=1-\exp\left(-\iint_{(r,\theta)\in\boldsymbol{S}}\mu_r P_u(r,\theta|R)\,r\mathrm{d}r\mathrm{d}\theta\right),\end{aligned} \quad (24)$$

where $\mathbb{N}_{\Psi_{R,u}}(\boldsymbol{S})$ denotes the number of Poisson points belonging to $\Psi_{R,u}$ that fall into region $\boldsymbol{S}$.

Eq. (24) shows that only RIS devices located inside $\boldsymbol{S}$ have influence on connection probability, where the boundary of $\boldsymbol{S}$ is $\partial\boldsymbol{S}$ such that the product of distances from points on $\partial\boldsymbol{S}$ to two fixed points $(\frac{1}{2}R,\pi)$ and $(\frac{1}{2}R,0)$ is a constant D_1. The illustration of $\partial\boldsymbol{S}$ is shown in Fig. 4. Herein, $\partial\boldsymbol{S}$ is a Cassini oval with parameters $a=\frac{1}{2}R$ and $b^2=D_1$. Cassini ovals are characterized by the fact that the product of the distances from points on the curve to two fixed points with distance $2a$ is equal to b^2. The polar equation of a Cassini oval is

$$\begin{cases}r=a\sqrt{\cos(2\theta)+\sqrt{(\frac{b}{a})^4-\sin^2(2\theta)}},\\ \qquad\qquad\theta\in[-\pi,\pi],\ \text{if } \frac{a}{b}\le 1\\ r=a\sqrt{\cos(2\theta)\pm\sqrt{(\frac{b}{a})^4-\sin^2(2\theta)}},\\ \qquad\theta\in[-\theta_0,\theta_0]\cup[\pi-\theta_0,\pi+\theta_0],\ \text{if } \frac{a}{b}>1\end{cases},$$

where $\theta_0=\frac{1}{2}\sin^{-1}[(\frac{b}{a})^2]$.

Substituting a with $\frac{1}{2}R$ and b with $\sqrt{D_1}$ in Eq. (25) leads to integral area in Eq. (24) and finally we get Lemma 3.

VI. Connection Probability of Multi-RIS Links

In this section, the upper bound of connection probability of multi-RIS links is derived for sparse obstacle distribution. The result is derived based on the connection probability of single-RIS links. To simplify analysis in this section, it is assumed that the receiver and the transmitter are located at $(0,0)$ and $(R,0)$ in polar coordinates, respectively. Let RIS1 denote the RIS device connected to the receiver in a M-RIS link as illustrated in Fig. 2(a).

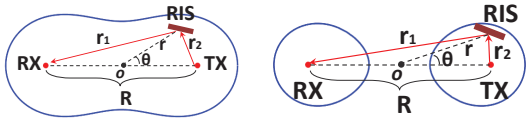

(a) $R\le 2\sqrt{D_1}$ (b) $R>2\sqrt{D_1}$

Fig. 4. Illustration of the boundary of eligible RIS device locations

In this section, Lemma 6 shows the upper bound for connection probability of multi-RIS links with sparse obstacle distribution. Lemma 4 and Lemma 5 provide preliminary conclusions used to derive Lemma 6.

For ease of derivation, we define two events as follows:

Event $A_M(D_M)$*: there exists at least one M-RIS path in a given domain* $\boldsymbol{H}$ *that can provide adequate received power. In other words, there is at least one M-RIS path that the product of (M+1) path segments is less than or equal to* D_M*, where* D_M *is defined in Sec. IV-B2. Note that* $P_M(D_M|R)=P(A_M(D_M))$.

Event $A_M(D_M,\boldsymbol{h}_i)$*: there exists at least one M-RIS path in a given domain* $\boldsymbol{H}$ *that can provide adequate received power (which means that the product of (M+1) path segments is less than or equal to* D_M*), and RIS1 is located in* $\boldsymbol{h}_i$ *with polar coordinate* (r_i,θ_i) *which is a subset of* $\boldsymbol{H}$ *and* $|\boldsymbol{h}_i|\to 0$.

Lemma 4 (Connection probability given the first RIS device location): For a transmitter and receiver pair at a distance R, if RIS1 which is the first RIS (as illustrated in Fig. 2(a)) in the M-RIS link is located at $\boldsymbol{h}_i=(r_i,\theta_i)$, the probability that the transmitter can communicate with the receiver with adequate received power via such M-RIS links (event $A_M(D_M,\boldsymbol{h}_i)$) is given by

$$\begin{aligned}P(A_M(D_M,\boldsymbol{h}_i))=\frac{1}{2}\mu_r|\boldsymbol{h}_i|e^{-(\beta_o+\beta_r)r_i-(p_o+p_r)}\times\\ P_{M-1}(\frac{D_M}{r_i}|\sqrt{r_i^2+R^2-2Rr_i\cos\theta_i}).\end{aligned} \quad (25)$$

Proof 4: The conditions of event $A_M(D_M,\boldsymbol{h}_i)$ occurring include occurrence of the following four events:

1) Event I_1^i: there is an RIS device located at $\boldsymbol{h}_i=(r_i,\theta_i)$, and the probability of its occurrence is $\mu_r|\boldsymbol{h}_i|$.
2) Event I_2^i: there is a LoS link between RIS1 and RX, and the probability of its occurrence is $P_{los}(r_i)$ according to Eq. (4).
3) Event $I_{M-1}^i(\frac{D_M}{r_i})$: there is an (M-1)-RIS link between location $\boldsymbol{h}_i$ and TX such that the product of path segments in the entire path is less than or equal to D_M. Since the distance between RIS1 and TX is $\sqrt{r_i^2+R^2-2Rr_i\cos\theta_i}$ and distance between RIS1 and RX is r_i, the probability of the event $I_{M-1}^i(\frac{D_M}{r_i})$ occurring is $P_1(\frac{D_M}{r_i}|\sqrt{r_i^2+R^2-2Rr_i\cos\theta_i})$.
4) Event I_o^i: RIS1 has a proper orientation so that RX and RIS2 (the second RIS device in the M-RIS link as

illustrated in Fig. 2(a)) are located on the same side of RIS1. The probability of the event I_o^i occurring is $\frac{1}{2}$.

Since these events are independent with each other, we can then get the results in Eq. (25) by $P(A_M(D_M, \boldsymbol{h}_i)) = P(I_1^i)P(I_2^i)P(I_{M-1}^i(\frac{D_M}{r_i}))P(I_o^i)$.

Lemma 5 (Event correlation): For sparse obstacle distribution, correlation among events $A_M(D_M, \mathbf{h}_i)$ can be demonstrated by the following inequality

$$P(\bigcap_{i=1}^{N_h} \overline{A_M(D_M, \boldsymbol{h}_i)}) > \prod_{i=1}^{N_h} P(\overline{A_M(D_M, \boldsymbol{h}_i)}). \tag{26}$$

Remark: The correlation among events $A_M(D_M, \mathbf{h}_i)$ is intractable to be quantified, which prevents the derivation of precise connection probability for multi-RIS links. But the above inequality can be used to derive an upper bound of M-RIS link connection probability for sparse obstacle distribution. The proof is demonstrated in Appendix. A high-level explanation of Lemma 5 is that events $\overline{A_M(D_M, \boldsymbol{h}_i)}$ are positively correlated with each other. This is in line with the intuitive understanding that if there is no M-RIS link where the first RIS is located at $\boldsymbol{h}_i$, then the probability of there being no M-RIS links starting from a location near $\boldsymbol{h}_i$ would increase.

Lemma 6 (Upper bound of connection probability of multi-RIS links): For a sparse obstacle distribution and a given pair of transmitter and receiver with distance R, the upper bound of connection probability of M-RIS links ($M \geq 2$) is

$$P_M^u(D_M|R) = \begin{cases} 1 - \exp\left(-\frac{1}{2}\mu_r \int_0^{2\pi}\int_0^{\infty} e^{-(\beta_o+\beta_r)r-(p_o+p_r)} \times \right. \\ \left. P_{M-1}^u(\frac{D_M}{r}|\sqrt{r^2+R^2-2Rr\cos\theta})r\,\mathrm{d}r\,\mathrm{d}\theta\right), \text{ if } M>2, \\ 1 - \exp\left(-\frac{1}{2}\mu_r \int_0^{2\pi}\int_0^{\infty} e^{-(\beta_o+\beta_r)r-(p_o+p_r)} \times \right. \\ \left. P_1(\frac{D_2}{r}|\sqrt{r^2+R^2-2Rr\cos\theta})r\,\mathrm{d}r\,\mathrm{d}\theta\right), \text{ if } M=2. \end{cases} \tag{27}$$

Proof 6: In order to derive the probability of occurrence of event $A_M(D_M)$, domain $\boldsymbol{H}$ can be separated into N_h disjoint subsets such that $\boldsymbol{H} = \bigcup_{i=1}^{N_h} \boldsymbol{h}_i$, $|\boldsymbol{h}_i| \to 0$ subject to the condition that $\boldsymbol{h}_i \cap \boldsymbol{h}_j = \emptyset$ if $i \neq j$. Then it can be concluded that $A_M(D_M) = \bigcup_{i=1}^{N_h} A_M(D_M, \boldsymbol{h}_i)$. Therefore,

$$\begin{aligned} P_M(D_M|R) &= 1 - P(\overline{A_M(D_M)}) \\ &= 1 - P(\bigcap_{i=1}^{N_h} \overline{A_M(D_M, \boldsymbol{h}_i)}). \end{aligned} \tag{28}$$

According to Lemma 5, it can be derived that the upper bound of Eq. (28) is as follows

$$P_M(D_M|R) < 1 - \prod_{i=1}^{N_h} P(\overline{A(D_M, \boldsymbol{h}_i)}) \tag{29}$$

$$\begin{aligned} &= 1 - \prod_{i=1}^{N_h} \exp\left(-\frac{1}{2}\mu_r |\boldsymbol{h}_i| e^{-(\beta_o+\beta_r)r_i-(p_o+p_r)} \times \right. \\ &\quad \left. P_{M-1}(\frac{D_M}{r_i}|\sqrt{r_i^2+R^2-2Rr_i\cos\theta_i})\right) \end{aligned} \tag{30}$$

$$\begin{aligned} &= 1 - \exp\left(-\frac{1}{2}\mu_r \int_0^{2\pi}\int_0^{\infty} e^{-(\beta_o+\beta_r)r-(p_o+p_r)} \times \right. \\ &\quad \left. P_{M-1}(\frac{D_M}{r}|\sqrt{r^2+R^2-2Rr\cos\theta})r\,\mathrm{d}r\,\mathrm{d}\theta\right). \end{aligned} \tag{31}$$

TABLE I
SIMULATION PARAMETERS

Parameters	Notations	Values
Carrier frequency	f_c	60 GHz
Equivalent isotropically radiated power (EIRP) for TX	$(P_tG_t)_{dBm}$	43 dBm
Received power threshold	P_{th}	-59 dBm
Antenna gain of users	G_r	11 dB

VII. NUMERICAL RESULTS

In Sec. VII-A, simulation results are provided to validate: (1) the connection probability of single-RIS links presented in Lemma 3, and (2) the upper bound of connection probability of multi-RIS links from Lemma 6. Next, in Sec. VII-B, a comparison of the coverage improvement using single-RIS links and two-RIS links is provided based on the approximated overall connection probability presented in Eq. (11). Herein, two-RIS links are considered as a representative case for multi-RIS scenarios, since multi-RIS links with more RIS devices could suffer practical issues of heavy overhead resulting from beam alignment and routing. For all results in this section, the link budget parameters are listed in Table I. Herein, an indoor mmWave LAN scenario operating at 60 GHz is simulated. The obstacle size is selected to model typical indoor objects, such as furniture. Therefore, the obstacle length and width are assumed to be uniform random variables with ranges [0.8 m, 1.2 m] and [0.4 m, 0.6 m], respectively. Moreover, the width and length of the RIS devices are chosen as $W_r = 0.05$ m, and $L_r = \sqrt{N_k}\frac{\lambda}{2}$, where λ is the wavelength and N_k is the number of RIS elements on one square RIS array. Let R denote the distance between the transmitter and the receiver. Then $R = 30$ m and $R = 150$ m are chosen to represent short-distance and long-distance communication, respectively.

A. Validation of connection probabilities

In this section, the analysis of single-RIS links from Lemma 3 and multi-RIS links from Lemma 6 are compared to simulation results. Two obstacle densities are studied: $\mu_o = 0.05/m^2$ and $\mu_0 = 0.01/m^2$, and primarily two RIS device densities are studied: $\mu_r = 0.005/m^2$ and $\mu_r = 0.001/m^2$. Later, we

will show that connection probability for $R = 150m$ and $\mu_o = 0.05/m^2$ is extremely low with these RIS densities so we add an RIS density $\mu_r = 0.03/m^2$ for that specific case.

Fig. 5 shows the relationship between RIS size and connection probability for single-RIS links for two different transmitter-receiver distances. The very slight gap in the figure between the theoretical analysis and simulation results indicates that the approximated connection probability in Lemma 3 provides a very good approximation. Note this is true both for a sparse obstacle scenario ($\mu_o = 0.01/m^2$) and a much denser obstacle scenario ($\mu_o = 0.05/m^2$). For RIS sizes that are practical with current technology (e.g., 32x32 to 64x64), the single-RIS link connection probability is good for the shorter distance but not very good for the longer distance. At the shorter distance, when the obstacle density is high ($\mu_o = 0.05/m^2$), it is effective to increase RIS device density to produce a good connection probability. However, increasing RIS size by itself results in a plateau of connection probability. At the longer distance, single-RIS links hardly provide any benefits with a dense obstacle distribution ($\mu_o = 0.05/m^2$) even if the RIS density increases to $\mu_r = 0.03/m^2$.

For the same two distances, Fig. 6 shows the relationship between RIS size and connection probability for two-RIS links, where the theoretical curve is the approximated upper bound on connection probability derived in Lemma 6. As compared to Fig. 5, the gap between theoretical analysis and simulation is slightly larger here. Note that the correlation between different links' LoS statuses, which is ignored in the upper bound analysis, sometimes *increases* the connection probability, which is why some of the simulated points appear above the approximated upper bound in the bottom blue curve in Fig. 6(a). This indicates that the sparse obstacle distribution assumption is violated at the higher obstacle density ($\mu_o = 0.05/m^2$). Nevertheless, the approximated upper bound and the simulation results still match quite closely in all cases for the obstacle densities studied. At the longer distance, two-RIS links provide significant connection probability improvement with a sparse obstacle distribution ($\mu_o = 0.01/m^2$). This highlights the effectiveness of two-RIS links compared with single-RIS links. When obstacle distribution is denser ($\mu_o = 0.05/m^2$), two-RIS links still show better connection probability in longer-distance communication compared with single-RIS links, especially with higher RIS density ($\mu_r = 0.03/m^2$). Nonetheless, the RIS benefit is only achieved with large RIS arrays (e.g., 96×96 and 128×128).

According to Fig. 5 and Fig. 6, both single-RIS and two-RIS links can provide significant connection probability with sparse obstacle distribution if RIS sizes and densities are appropriately chosen. Moreover, from Fig. 5(a) and Fig. 6(a), we see that single-RIS links provide better connection probability than two-RIS links for short-distance transmissions. However, in comparing Fig. 5(b) and Fig. 6(b), note that two-RIS links gradually outperform single-RIS links for longer-distance transmissions as RIS size increases. As RIS size increases, the larger gain allows the longer two-RIS links to meet the required received power threshold and since two-RIS links provide more opportunity for blockage avoidance, they outperform single-RIS links in that situation.

B. Overall connection probability improvement

In this section, the approximated overall connection probability in Eq. (11) is investigated for a more comprehensive analysis of coverage improvement with RIS links. Note that connection probability of single-RIS links in Lemma 3 and upper bound for two-RIS links according to Lemma 6 are used to approximate the overall connection probability. Herein, single-RIS systems are defined as systems that can support the LoS link and single-RIS links, while two-RIS systems can support the LoS link, single-RIS links, and two-RIS links. Simulation results and theoretical analyses are shown in Fig. 7. In this section, we focus on the case where $\mu_o = 0.01/m^2$ and $\mu_r = 0.001/m^2$, so the sparse obstacle assumption holds.

In Fig. 7, despite the gap between theoretical analysis and simulation results, the theoretical connection probability still provides beneficial insights into comparison between single-RIS and two-RIS systems. First, for the link budget parameters used in this simulation, small-sized RISs (i.e., RISs with 16×16 elements) do not provide any connection probability improvement compared with LoS communication due to the limited RIS gain. Second, for shorter transmission distances (Fig. 7(a)), single-RIS systems can achieve perfect connection probability with sufficiently large RIS sizes. Meanwhile, two-RIS systems hardly produce any improvement in this case, indicating the effectiveness and efficiency of single-RIS systems for short-range communication. However, for longer-distance communication (Fig. 7(b)), two-RIS systems have a significant advantage compared to single-RIS systems. According to Fig. 7(b), when RIS size is 80×80 or larger, two-RIS systems show nearly twice the improvement in overall connection probability compared to single-RIS systems.

VIII. Conclusion

In this paper, the connection probability of multi-RIS communication was analyzed theoretically. The single-RIS link connection probability and an upper bound on multi-RIS link connection probability were derived in sparse obstacle scenarios to allow investigation of the relationships among coverage performance, RIS and obstacle distributions. Monte Carlo simulations validated the theoretical analysis for single-RIS and two-RIS links and allowed us to compare the relative benefits of them. We found that it is efficient to use single-RIS links for short-distance communication while two-RIS links can improve coverage significantly for long-distance communication when medium to large sized RISs are deployed.

Appendix

Let $F^1_{D_m}(d) = P(\bigcap_{i=1}^{N} \overline{A_m(d, \boldsymbol{h}_i)})$ and $F^2_{D_m}(d) = \prod_{i=1}^{N} P(\overline{A_m(d, \boldsymbol{h}_i)})$, where D_m represents the threshold of the product of $(m+1)$ path segment lengths in an m-RIS link. To demonstrate that $F^1_{D_m}(d) > F^2_{D_m}(d)$, it suffices to show that $F^1_{D_m|\boldsymbol{\Theta}}(d|\theta) > F^2_{D_m|\boldsymbol{\Theta}}(d|\theta)$, where $\boldsymbol{\Theta}$ represents possible RIS orientations at all the locations.

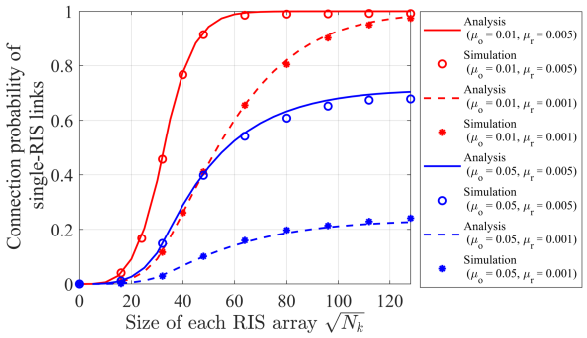

(a) Distance between TX and RX is 30 m

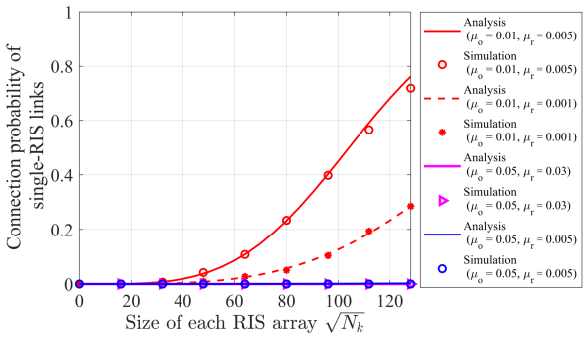

(b) Distance between TX and RX is 150 m

Fig. 5. Connection probability of single-RIS links vs. RIS size (number of elements on each RIS array is N_k)

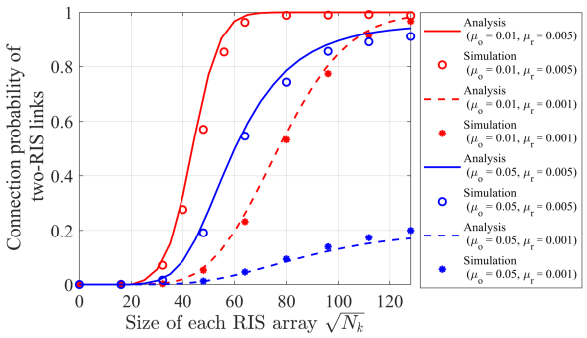

(a) Distance between TX and RX is 30 m

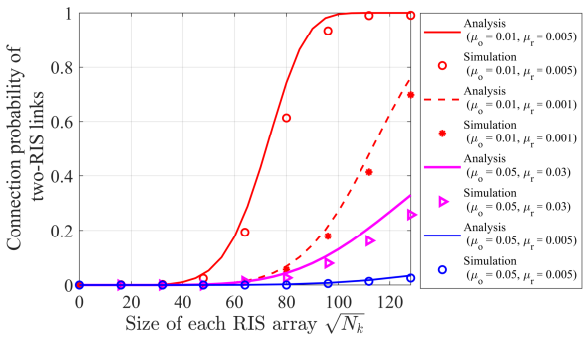

(b) Distance between TX and RX is 150 m

Fig. 6. Connection probability of two-RIS links vs. RIS size for indoor scenario (number of elements on each RIS array is N_k)

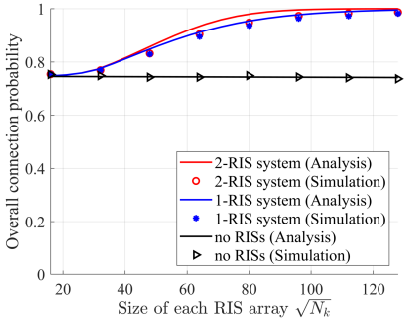

(a) Distance between TX and RX is 30 m

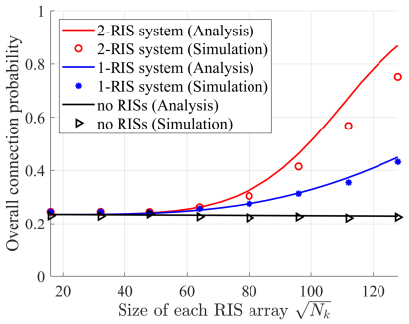

(b) Distance between TX and RX is 150 m

Fig. 7. Overall connection probability vs. RIS size for indoor scenario (number of elements on each RIS array is N_k, RIS density $\mu_r = 0.001/m^2$, and obstacle density $\mu_o = 0.01/m^2$)

Recall that $A_m(d, \mathbf{h}_i) = I_1^i \cap I_2^i \cap I_{m-1}^i(d/r_i) \cap I_o^i$. Let $R^i = I_1^i \cap I_2^i$ and $R_{m-1}^i(x_i) = I_{m-1}^i(x_i) \cap I_o^i$. Then $F_{D_m|\mathbf{\Theta}}^1(d|\theta)$ and $F_{D_m|\mathbf{\Theta}}^2(d|\theta)$ can be interpreted as follows

$$F_{D_m|\mathbf{\Theta}}^1(d|\theta) = \sum_{i=0}^{N} P(E_{m,i}^1|\theta), \tag{32}$$

where $E_{m,k}^1$ denote the event in which, among the N possible locations of RIS1, there are exactly k locations where event R^i occurs but event $R_{m-1}^i(\frac{d}{r_i})$ does not occurs, while none of the remaining $N-k$ locations exhibit the occurrence of R^i, such that

$$P(E_{m,i}^1|\theta) = \sum_{n_1=1}^{N-i+1} \sum_{n_2=n_1+1}^{N-i+2} \cdots \sum_{n_i=n_{i-1}+1}^{N} \prod_{k\in \{n_1,n_2,\ldots,n_i\}} P(R^k) \prod_{\substack{l=1,\\ l\notin\{n_1,n_2,\ldots,n_i\}}}^{N} P(\overline{R^l}) P\Big(\bigcap_{j\in\{n_1,n_2,\ldots,n_i\}} \overline{R_{m-1}^j(\frac{d}{r_j})}|\theta\Big). \tag{33}$$

If independence of events $\overline{A_M(d, \boldsymbol{h}_i)}$ is assumed, we have

$$F_{D_m|\mathbf{\Theta}}^2(d|\theta) = \sum_{i=0}^{N} P(E_{m,i}^2|\theta), \tag{34}$$

where

$$P(E^2_{m,i}|\theta) = \sum_{n_1=1}^{N-i+1} \sum_{n_2=n_1+1}^{N-i+2} \cdots \sum_{n_i=n_{i-1}+1}^{N} \prod_{\substack{k\in \\ \{n_1,n_2,\ldots,n_i\}}} P(R^k) \prod_{\substack{l=1, \\ l\notin\{n_1,n_2,\ldots,n_i\}}}^{N_h} P(\overline{R^l}) \prod_{j\in\{n_1,n_2,\ldots,n_i\}} \overline{P(R^j_{m-1}(\frac{d}{r_j})|\theta)}. \quad (35)$$

The event $\bigcap_{j\in\mathbf{Q}} \overline{R^j_m(x_j)}|\theta$ can be interpreted as the event that, considering possible RIS orientations θ, there are no proper m-RIS links between TX and each location $\mathbf{h}_j$ where $j \in \mathbf{Q}$. By comparing Eq. (33) and Eq. (35), we need to show that $P(\bigcap_{j\in\mathbf{Q}} \overline{R^j_{m-1}(x_j)}|\theta) > \prod_{j\in\mathbf{Q}} P(\overline{R^j_{m-1}(x_j)}|\theta)$ in order to demonstrate that $F^1_{D_m|\mathbf{\Theta}}(d|\theta) > F^2_{D_m|\mathbf{\Theta}}(d|\theta)$.

We will start from $m = 2$, such that

$$P(\bigcap_{j\in\mathbf{Q}} \overline{R^j_1(x_j)}|\theta) = \prod_{k=1}^{N_h} e^{-\lambda|h_k|P(\bigcup_{j\in\mathbf{Q}^k_\theta} H^1_{j,k}(x_j))}, \quad (36)$$

where N_h denotes the total number of possible RIS locations in a given domain, and $\mathbf{Q}^k_\theta \subset \mathbf{Q}$ denotes the subset of indexes of locations in $\mathbf{Q}$ that can provide proper RIS orientations to form a 1-RIS link between RX and location $\mathbf{h}_k$ considering possible RIS locations θ. Moreover, $H^m_{j,k}(x_j)$ represents the event that there exists a proper m-RIS link between location $\mathbf{h}_j$ and TX, and the first RIS connected to $\mathbf{h}_j$ is located at $\mathbf{h}_k$.

If events $\overline{R^j_1(x_j)}$ are independent with each other, then

$$\prod_{j\in\mathbf{Q}} P(\overline{R^j_1(x_j)}|\theta) = \prod_{k=1}^{N_h} e^{-\lambda|h_k|P(\sum_{j\in\mathbf{Q}^k_\theta} H^1_{j,k}(x_j))} < \prod_{k=1}^{N_h} e^{-\lambda|h_k|P(\bigcup_{j\in\mathbf{Q}^k_\theta} H^1_{j,k}(x_j))}. \quad (37)$$

Then we have $P(\bigcap_{j\in\mathbf{Q}} \overline{R^j_1(x_j)}|\theta) > \prod_{j\in\mathbf{Q}} P(\overline{R^j_1(x_j)}|\theta)$ for $m = 2$. When $m > 2$, a similar way of interpreting $F^1_{D_m|\mathbf{\Theta}}(d|\theta)$ and $F^2_{D_m|\mathbf{\Theta}}(d|\theta)$ can be used to show that the relationship between $P(\bigcap_{j\in\mathbf{Q}} \overline{R^j_{m-1}(x_j)}|\theta)$ and $\prod_{j\in\mathbf{Q}} P(\overline{R^j_{m-1}(x_j)}|\theta)$ depends on the relationship between $P(\bigcap_{j\in\mathbf{Q}} \overline{R^j_{m-2}(x_j)}|\theta)$ and $\prod_{j\in\mathbf{Q}} P(\overline{R^j_{m-2}(x_j)}|\theta)$. Since it is demonstrated that $P(\bigcap_{j\in\mathbf{Q}} \overline{R^j_1(x_j)}|\theta) > \prod_{j\in\mathbf{Q}} P(\overline{R^j_1(x_j)}|\theta)$, then we have $P(\bigcap_{j\in\mathbf{Q}} \overline{R^j_{m-1}(x_j)}|\theta) > \prod_{j\in\mathbf{Q}} P(\overline{R^j_{m-1}(x_j)}|\theta)$ for $m \geq 2$. In other words, it indicates that $F^1_{D_m|\mathbf{\Theta}}(d|\theta) > F^2_{D_m|\mathbf{\Theta}}(d|\theta)$.

REFERENCES

[1] T. Bai and R. W. Heath, "Coverage and rate analysis for millimeter-wave cellular networks," *IEEE Transactions on Wireless Communications*, vol. 14, no. 2, pp. 1100–1114, 2015.

[2] Y. Liu, Y. Jian, R. Sivakumar, and D. M. Blough, "Optimal access point placement for multi-ap mmwave wlans," in *Proceedings of the 22nd International ACM Conference on Modeling, Analysis and Simulation of Wireless and Mobile Systems*, 2019, pp. 35–44.

[3] Y. Yan, Q. Hu, and D. M. Blough, "Path selection with amplify and forward relays in mmwave backhaul networks," in *2018 IEEE 29th Annual International Symposium on Personal, Indoor and Mobile Radio Communications (PIMRC)*. IEEE, 2018, pp. 1–6.

[4] Q. Hu and D. M. Blough, "Relay selection and scheduling for millimeter wave backhaul in urban environments," in *2017 IEEE 14th International Conference on Mobile Ad Hoc and Sensor Systems (MASS)*, 2017, pp. 206–214.

[5] A. Deng, Y. Liu, and D. M. Blough, "Maximizing coverage for mmwave wlans with dedicated reflectors," in *ICC 2021-IEEE International Conference on Communications*. IEEE, 2021, pp. 1–6.

[6] J. Zhang and D. M. Blough, "Optimizing coverage with intelligent surfaces for indoor mmwave networks," in *IEEE INFOCOM 2022 - IEEE Conference on Computer Communications*, 2022, pp. 830–839.

[7] J. Zhang and D. M. Blough, "Optimal placement of reconfigurable intelligent surfaces with random obstacle distribution," in *2023 IEEE Wireless Communications and Networking Conference (WCNC)*, 2023, pp. 1–6.

[8] Q. Wu and R. Zhang, "Towards smart and reconfigurable environment: Intelligent reflecting surface aided wireless network," *IEEE Communications Magazine*, vol. 58, no. 1, pp. 106–112, 2019.

[9] Y. Cao, T. Lv, and W. Ni, "Intelligent reflecting surface aided multi-user mmwave communications for coverage enhancement," in *2020 IEEE 31st Annual International Symposium on Personal, Indoor and Mobile Radio Communications*, 2020, pp. 1–6.

[10] G. Lee, M. Jung, A. T. Z. Kasgari, W. Saad, and M. Bennis, "Deep reinforcement learning for energy-efficient networking with reconfigurable intelligent surfaces," in *ICC 2020 - 2020 IEEE International Conference on Communications (ICC)*, 2020, pp. 1–6.

[11] V. K. Chapala and S. M. Zafaruddin, "Reconfigurable intelligent surface empowered multi-hop transmission over generalized fading," in *2022 IEEE 95th Vehicular Technology Conference: (VTC2022-Spring)*, 2022, pp. 1–5.

[12] M. Di Renzo and J. Song, "Reflection probability in wireless networks with metasurface-coated environmental objects: an approach based on random spatial processes," *EURASIP Journal on Wireless Communications and Networking*, vol. 2019, no. 1, p. 99, Apr 2019. [Online]. Available: https://doi.org/10.1186/s13638-019-1403-7

[13] M. A. Kishk and M. S. Alouini, "Exploiting randomly located blockages for large-scale deployment of intelligent surfaces," *IEEE Journal on Selected Areas in Communications*, vol. 39, no. 4, pp. 1043–1056, 2021.

[14] W. Tang, M. Z. Chen, X. Chen, J. Y. Dai, Y. Han, M. Di Renzo, Y. Zeng, S. Jin, Q. Cheng, and T. J. Cui, "Wireless communications with reconfigurable intelligent surface: Path loss modeling and experimental measurement," *IEEE Transactions on Wireless Communications*, vol. 20, no. 1, pp. 421–439, 2021.

[15] E. Björnson, Ö. T. Demir, and L. Sanguinetti, "A primer on near-field beamforming for arrays and reconfigurable intelligent surfaces," in *2021 55th Asilomar Conference on Signals, Systems, and Computers*. IEEE, 2021, pp. 105–112.

[16] S. Hu, M. C. Ilter, and H. Wang, "Near-field beamforming for large intelligent surfaces," in *2022 IEEE 33rd Annual International Symposium on Personal, Indoor and Mobile Radio Communications (PIMRC)*, 2022, pp. 1367–1373.

[17] T. Bai, R. Vaze, and R. W. Heath, "Analysis of blockage effects on urban cellular networks," *IEEE Transactions on Wireless Communications*, vol. 13, no. 9, pp. 5070–5083, 2014.

[18] T. Shafique, H. Tabassum, and E. Hossain, "Stochastic geometry analysis of irs-assisted downlink cellular networks," *IEEE Transactions on Communications*, vol. 70, no. 2, pp. 1442–1456, 2022.

[19] W. Mei and R. Zhang, "Multi-beam multi-hop routing for intelligent reflecting surfaces aided massive mimo," *IEEE Transactions on Wireless Communications*, vol. 21, no. 3, pp. 1897–1912, 2022.

[20] P. A. W. Lewis and G. S. Shedler, "Simulation of nonhomogeneous poisson processes by thinning," *Naval Research Logistics Quarterly*, vol. 26, no. 3, pp. 403–413, 1979. [Online]. Available: https://onlinelibrary.wiley.com/doi/abs/10.1002/nav.3800260304